

Solid-liquid transition induced by the anisotropic diffusion of colloidal particles

Fu-Jun Lin(蔺福军), Jing-Jing Liao(廖晶晶), Jian-Chun Wu(吴建春), and Bao-Quan Ai(艾保全)
Citation: Chin. Phys. B, 2022, 31 (**3**): 036401. DOI: 10.1088/1674-1056/ac1e19
Journal homepage: http://cpb.iphy.ac.cn; http://iopscience.iop.org/cpb

What follows is a list of articles you may be interested in

Novel structures and mechanical properties of Zr_2N: *Ab initio* description under high pressures

Minru Wen(文敏儒), Xing Xie(谢兴), Zhixun Xie(谢植勋), Huafeng Dong(董华锋), Xin Zhang(张欣), Fugen Wu(吴福根), and Chong-Yu Wang(王崇愚)
Chin. Phys. B, 2021, 30 (**1**): 016403. DOI: 10.1088/1674-1056/abb220

Temperature-induced phase transition of two-dimensional semiconductor GaTe

Xiaoyu Wang(王啸宇), Xue Wang(王雪), Hongshuai Zou(邹洪帅), Yuhao Fu(付钰豪), Xin He(贺欣), and Lijun Zhang(张立军)
Chin. Phys. B, 2021, 30 (**1**): 016402. DOI: 10.1088/1674-1056/abd394

Growth and structural characteristics of metastable β-In_2Se_3 thin films on H-terminated Si(111) substrates by molecular beam epitaxy

Yi-Fan Shen(沈逸凡), Xi-Bo Yin(尹锡波), Chao-Fan Xu(徐超凡), Jing He(贺靖), Jun-Ye Li(李俊烨), Han-Dong Li(李含冬), Xiao-Hong Zhu(朱小红), Xiao-Bin Niu(牛晓滨)
Chin. Phys. B, 2020, 29 (**5**): 056402. DOI: 10.1088/1674-1056/ab820f

Structural transitions in $NaNH_2$ via recrystallization under high pressure

Yanping Huang(黄艳萍), Xiaoli Haung(黄晓丽), Xin Wang(王鑫), Wenting Zhang(张文亭), Di Zhou(周迪), Qiang Zhou(周强), Bingbing Liu(刘冰冰), Tian Cui(崔田)
Chin. Phys. B, 2019, 28 (**9**): 096402. DOI: 10.1088/1674-1056/ab37f8

Crystal melting processes of propylene carbonate and 1,3-propanediol investigated by the reed-vibration mechanical spectroscopy for liquids

Li-Na Wang(王丽娜), Xing-Yu Zhao(赵兴宇), Heng-Wei Zhou(周恒为), Li Zhang(张丽), Yi-Neng Huang(黄以能)
Chin. Phys. B, 2019, 28 (**9**): 096401. DOI: 10.1088/1674-1056/ab327d

---

Solid-liquid transition induced by the anisotropic diffusion of colloidal particles

Fu-Jun Lin(蔺福军)[1,2], Jing-Jing Liao(廖晶晶)[2], Jian-Chun Wu(吴建春)[1], and Bao-Quan Ai(艾保全)[1,†]

[1] *Guangdong Provincial Key Laboratory of Quantum Engineering and Quantum Materials, Guangdong-Hong Kong Joint Laboratory of Quantum Matter, School of Physics and Telecommunication Engineering, South China Normal University, Guangzhou* 510006, *China*
[2] *School of Science, Jiangxi University of Science and Technology, Ganzhou* 341000, *China*

(Received 11 May 2021; revised manuscript received 7 July 2021; accepted manuscript online 17 August 2021)

We numerically study the phase behaviors of colloids with anisotropic diffusion in two dimensions. It is found that the diffusion anisotropy of colloidal particles plays an important role in the phase transitions. A strong diffusion anisotropy induces the large vibration of particles, subsequently, the system goes into a disordered state. In the presence of the strong-coupling, particles with weak diffusion anisotropy can freeze into hexagonal crystals. Thus, there exists a solid-liquid transition. With the degree of diffusion anisotropy increasing, the transition points are shifted to the stronger-coupled region. A competition between the degree of diffusion anisotropy and coupling strength widens the transition region where the heterogeneous structures coexist, which results in a broad-peak probability distribution curve for the local order parameter. Our study may be helpful for the experiments related to the phase behavior in statistical physics, materials science and biophysical systems.

Keywords: phase transition, anisotropic diffusion, colloidal particles

PACS: 64.70.pv, 05.70.–a, 47.51.+a **DOI:** 10.1088/1674-1056/ac1e19

1. Introduction

Phase transition is ubiquitous in nature as well as in industry, and plays an essential role in statistical physics, materials science, chemistry, and biophysics. Physicists and mathematicians have long been fascinated by this issues. Understanding the phase transition kinetics and microscale processes is important not only for fundamental research, but also for applications associated with crystalline materials[1] and biotechnology.[2,3] Quantitative examinations on phase transition are mostly based on the models of repulsive hard spheres (discs),[4–8] charged spheres,[9–11] or attractive spheres.[12,13] As everyone knows, it is challenging experimentally to investigate the particles dynamics on an atomic or molecular scale. The colloidal particles, dispersing in a fluid medium, are larger than solvent molecules, but small enough to undergo Brownian motion. They are usually viewed as large atoms with tailorable sizes, shapes and interactions,[14] their thermal motion can be visualized by optical microscopy[15] and tracked by image processing.[16] Therefore, the colloidal suspensions have always been examined to understand the physical phenomena such as freezing, nucleation, melting, phase separation, structure formation, either spontaneous or driven by external fields.[17–22] The potential application of the spontaneous self-assembled of colloids can be selected as a promising route for fabrication of nanostructures, which requires us to deeply understand the relationship between their properties, structures and the self-organization processes.

The systematic studies mostly focus on the phase transition of the colloidal particles. Crystallization represents the prime example of a liquid-solid transition and has been extensively examined in many cases. Numerous types of crystals were revealed in simulations and experiments. A flowing crystalline structure, named rheocrystal, can spontaneously form by removing the particles, which is supported by numerical simulation and experiment.[23] However, a Monte Carlo 'constrained aging' method slows crystallization.[24] It is worth mentioning that an excellent work on crystallization of monodisperse self-propelled colloidal particles at sufficiently high densities has been carried out by Bialké *et al.*[18] They explored that the active colloids still freeze into a crystalline structure though the energy is injected incessantly, the freezing transition is largely shifted due to the self-propulsion. Furthermore, the phase behavior in a system of binary hard spheres with different sizes has been reported in experiments[25,26] and theory.[27–29] The results indicate that the small spheres can fit between large spheres to stabilize binary crystals. The basic mechanisms of melting, spinodal decomposition, nucleation, and the glasses transition were performed in the past decades.

Most of the works on phase transition mentioned above mainly focus on spherical isotropic particles. However, perfect symmetry is an ideal case in nature. The anisotropy of particles, including the shape (e.g., ellipsoids, rods, or cubes), interaction (e.g., janus) as well as diffusion anisotropy (e.g., po-

†Corresponding author. E-mail: aibq@scnu.edu.cn

© 2022 Chinese Physical Society and IOP Publishing Ltd

lar particles), is an intrinsic property. Specifically, anisotropic colloidal particles can be produced by tuning the shape of the particles, or putting the patches on the surface of the particles, also synthesized by two hemispheres with different properties. Indeed, studies on anisotropic particles have provided us with a wealth of insight into many microscopic kinetics and physical phenomena. The needle-like ellipsoidal particles under the action of an external potential exhibit complex motion and destroy the directed transport.[30,31] A variety of crystalline structures have been discovered by varying the shape anisotropy of spheroids.[32] However, phase transition behavior of spherical anisotropic particles has rarely been studied. In this paper, we study phase behavior of colloids with anisotropic diffusion and focus on finding how the diffusion anisotropy affects the solid-liquid transition.

2. Model and methods

We consider a suspension of N particles with diffusion anisotropy in two dimensions under periodic boundary conditions. Due to the particle anisotropy, the rotational and translational motions are always coupled in the lab-frame coordinates, which makes the analysis of relevant issues very complicated. For simplicity, we initially describe the motion of particle in body-fixed coordinates where the rotational and translational motions are decoupled. Then, the particle's position vector $\boldsymbol{S}(t)$ of its center of mass at a given time t can be decomposed as $(\delta\tilde{x}, \delta\tilde{y})$, corresponding to the coordinates $(\delta x, \delta y)$ in the lab frame. Here, $\theta(t)$ is the angle between the x axis and the $\tilde{x}$ axis. By means of a straightforward rotation of coordinates and a series of manipulations, the overdamped motion of the i particle in Fig. 1(b) can be written as[33,34]

$$\begin{aligned}\frac{\partial x_i(t)}{\partial t} &= F_i^x\left[\bar{\mu}+\Delta\tilde{\mu}\cos(2\theta_i(t))\right] \\ &\quad +\Delta\tilde{\mu}F_i^y\sin(2\theta_i(t))+\eta_i^x(t), \qquad (1)\\ \frac{\partial y_i(t)}{\partial t} &= F_i^y\left[\bar{\mu}-\Delta\tilde{\mu}\cos(2\theta_i(t))\right] \\ &\quad +\Delta\tilde{\mu}F_i^x\sin(2\theta_i(t))+\eta_i^y(t), \qquad (2)\\ \frac{1}{\mu_3}\frac{\partial\theta_i(t)}{\partial t} &= \eta_i^\theta(t). \qquad (3)\end{aligned}$$

We have defined the mobilities along the $\tilde{x}$ and $\tilde{y}$ axes as μ_1 and μ_2, respectively, and the rotational mobility as μ_3. Here $\bar{\mu}=\frac{1}{2}(\mu_1+\mu_2)$ is the average of the mobility, and $\Delta\tilde{\mu}=\frac{1}{2}(\mu_1-\mu_2)$ determines the anisotropy of the particle, $\Delta\tilde{\mu}=0$ indicates that the particle is isotropic, and while $\Delta\tilde{\mu}\to\bar{\mu}$, the particle is prone to diffuse along the $\tilde{x}$ axis. F_i^x and F_i^y are the components of the force along the x and y axis of lab frame. For convenience, the energy, length and time are normalized by $k_BT, \rho^{-1/2}$ and $(\rho D_0)^{-1}$, respectively. Here, T is temperature, k_B is the Boltzman constant, ρ is the number density and D_0 is the bare diffusion coefficient. For a many-particle system, the particles are considered to interact pairwise through the repulsive Yukawa potential:[35] $u(r)=\Gamma\frac{e^{-\lambda r}}{r}$, with screening length λ^{-1}, and the dimensionless coupling strength $\Gamma\equiv V_0\sqrt{\rho}/k_BT$ using the bare potential strength V_0. Thus, the force acts on the i-th particle is $\boldsymbol{F}_i=-\nabla_i\sum_{i<j}u(|\boldsymbol{r}_i-\boldsymbol{r}_j|)$. The noise $\eta_i^m(t)$ in the lab frame has mean zero and satisfies[33,34]

$$\left\langle\eta_i^\theta(t)\eta_i^\theta(t')\right\rangle = 2D_\theta\delta\left(t-t'\right), \qquad (4)$$

$$\left\langle\eta_i^m(t)\eta_i^n(t')\right\rangle_{\theta_i(t)}^{\eta_i^x\eta_i^y} = 2k_BT\mu_{mn}\delta\left(t-t'\right),\ \ m,n=x,y, \qquad (5)$$

with

$$\mu_{mn}=\bar{\mu}\,\delta_{mn}+\Delta\tilde{\mu}\begin{pmatrix}\cos 2\theta & \sin(2\theta)\\ \sin 2\theta & -\cos(2\theta)\end{pmatrix}, \qquad (6)$$

where $D_\theta=k_BT\mu_3$ is the rotational diffusion coefficient, describing the angular fluctuation. The superscripts of statistical averages in Eq. (5) mean over which the noises are averaged, and the subscript quantity is kept fixed. Defining $\Delta\mu\equiv\Delta\tilde{\mu}/\bar{\mu}\in[0,1)$ to describe the anisotropy, the diffusion coefficient of the particle are $D_1=k_BT\mu_1$ and $D_2=k_BT\mu_2=[(1-\Delta\mu)/(1+\Delta\mu)]D_1$, respectively.

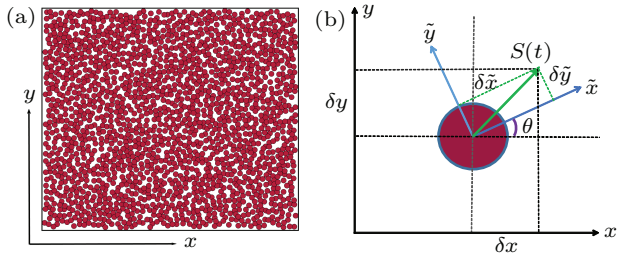


Fig. 1. Schematic diagram illustrating the setup forming the basis of our calculations. (a) Model of colloids moving in a two-dimensional box. (b) Representation of an anisotropic particle. The axes $\tilde{x}$ and $\tilde{y}$ are body-fixed coordinates, and the axes x and y are the lab-frame coordinates.

3. Numerical results and discussion

In our simulations, we choose $N=1936$, $D_\theta=3.0$, and $D_1=1.0$, $\lambda=3.5$. $L_x/L_y=2/\sqrt{3}$ is chosen for the particles can crystallize into the perfect hexagonal crystal. The initial position and orientation of particles are random. The integration time step dt is chosen to be smaller than 10^{-4} and the total integration time to be greater than 10^3, which ensures that the system reaches a steady state and the simulation results will not depend on the integration time and time step.

The structural transitions between the different phases can be characterized by the global bond-orientational order parameter[36]

$$\psi_6\equiv\left\langle\left|\frac{1}{N}\sum_{i=1}^{N}q_6(i)\right|^2\right\rangle,\quad q_6(i)\equiv\frac{1}{6}\sum_{j\in\Pi(i)}e^{i6\theta_{ij}}, \qquad (7)$$

where $\Pi(i)$ is the set of the six nearest neighbors of the ith particle and θ_{ij} is the angle between the vector from particle i to j and an predefined direction. For a perfect crystal $\psi_6 = 1$, whereas $\psi_6 \to 0$ in a disordered phase. Following Schweigert *et al.*,[37] the liquid-to-solid transition can be identified by a jump of the order parameter above a value of $\psi_6 \cong 0.45$. Meanwhile, a dynamical criterion for phase transition of the particles is determined by the abrupt drop of the long-time diffusion coefficient

$$D \equiv \lim_{t\to\infty} \frac{1}{4} \left\langle |\Delta \boldsymbol{r}_i(t)|^2 \right\rangle, \tag{8}$$

with $\Delta \boldsymbol{r}_i(t) = \boldsymbol{r}_i(t) - \boldsymbol{r}_i(0)$. The value of 0.086 for D has been proved by Löwen to be 'universal', regardless of whether freezing occurs continuously via a hexagonal phase or is a conventional first-order transition,[38] thus we employ this criterion to describe the dynamical phase transition.

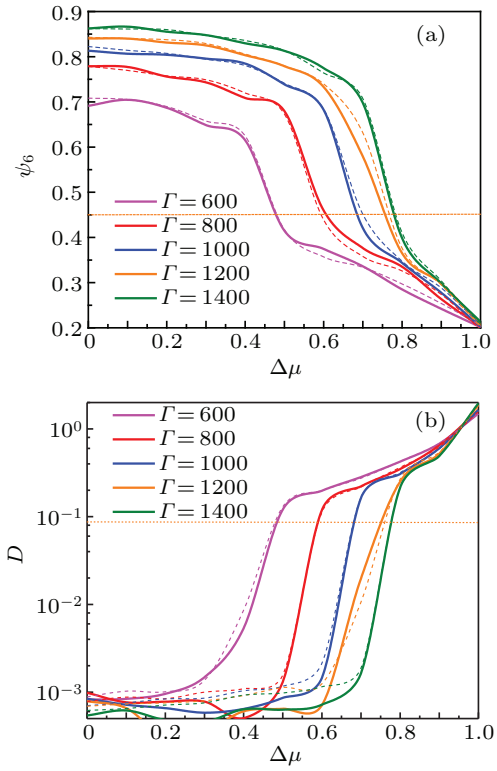


Fig. 2. Cooling curves (solid lines) and melting curves (dashed lines) for (a) the bond-orientational parameter ψ_6 and (b) the long-time diffusion coefficient D versus the degree of diffusion anisotropy $\Delta\mu$ for different Γ. The crossings with the dashed horizontal lines define the position of the structural transition $\Delta\mu_S^*$ ($\psi_6 = 0.45$) and the dynamical freezing $\Delta\mu_D^*$ ($D = 0.086$), respectively.

We firstly examine the effect of the degree of diffusion anisotropy $\Delta\mu$ on the phase transition by monitoring the global bond-orientational order parameter ψ_6 and the long-time diffusion coefficient D for different Γ in Fig. 2. At the beginning of the simulation, a particle configuration with random particle positions and orientations is employed. From Fig. 2(a) we find that for a given Γ, the particles can freeze into an ordered crystalline phase in the small $\Delta\mu$ region, especially for isotropic particles ($\Delta\mu = 0$), ψ_6 has its maximum value. With increasing $\Delta\mu$, the Brownian diffusion along a specific axis of a particle becomes increasingly dominant, the random motion hinders the system from assembling an ordered structure. Therefore, the order parameter drops to below $\psi_6 = 0.45$ at $\Delta\mu \equiv \Delta\mu_S^*$, indicating a loss of the long-range orientational order in the system, and the system transits into the liquid phase.[39] Figure 2(b) exhibits dynamical phase transition for different Γ, the diffusion coefficient increases abruptly near the phase transition point $\Delta\mu_D^*$, which gives the lower bound to liquid region, and even exceeds that of a free passive Brownian particle. Obviously, the phase transition point is significantly shifted to the large Γ region, which is determined by the competition between the degree of diffusion anisotropy and the coupling strength. As shown in Fig. 3, with increasing Γ, the corresponding temperature of the system decreases, which leads to the dense colloids to gradually freeze into an ordered configuration and the diffusion coefficient to drop toward zero.

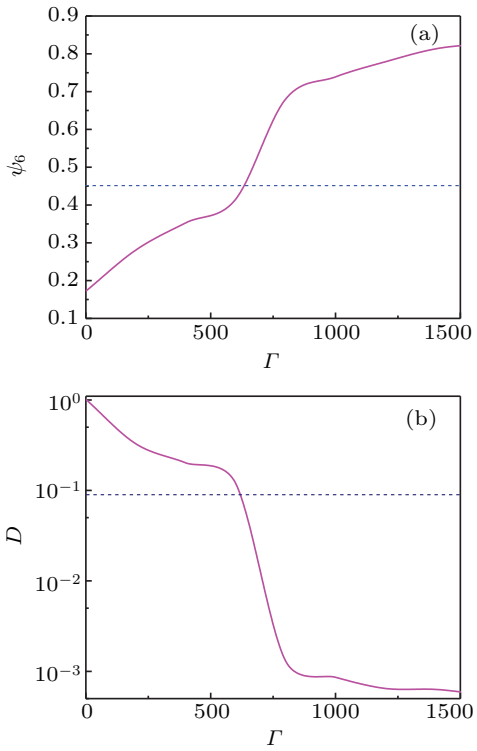


Fig. 3. Cooling curves for (a) the bond-orientational parameter ψ_6 and (b) the long-time diffusion coefficient D versus coupling strength Γ at $\Delta\mu = 0.5$.

To effectively distinguish liquid-like from ordered regions, we utilize an order parameter $\bar{q}_6 \equiv \mathrm{Re}\sum_{j\in\Pi(i)} \frac{1}{6}\sum q_6(i) q_6^*(j)$ per particle to describe the local behavior of its neighbors.[40] The snapshots of particle configurations for $\Delta\mu = 0$, 0.5 and 0.9 with different Γ are illustrated in Fig. 4. Clearly, for either small coupling strength (e.g., $\Gamma = 200$) or large diffusion anisotropic degree (e.g., $\Delta\mu = 0.9$), the system always stays liquid with small order parameter. However, for the isotropic particles ($\Delta\mu = 0$), the system crystallizes into hexagonal structures with $\psi_6 > 0.8$ under low temperature.

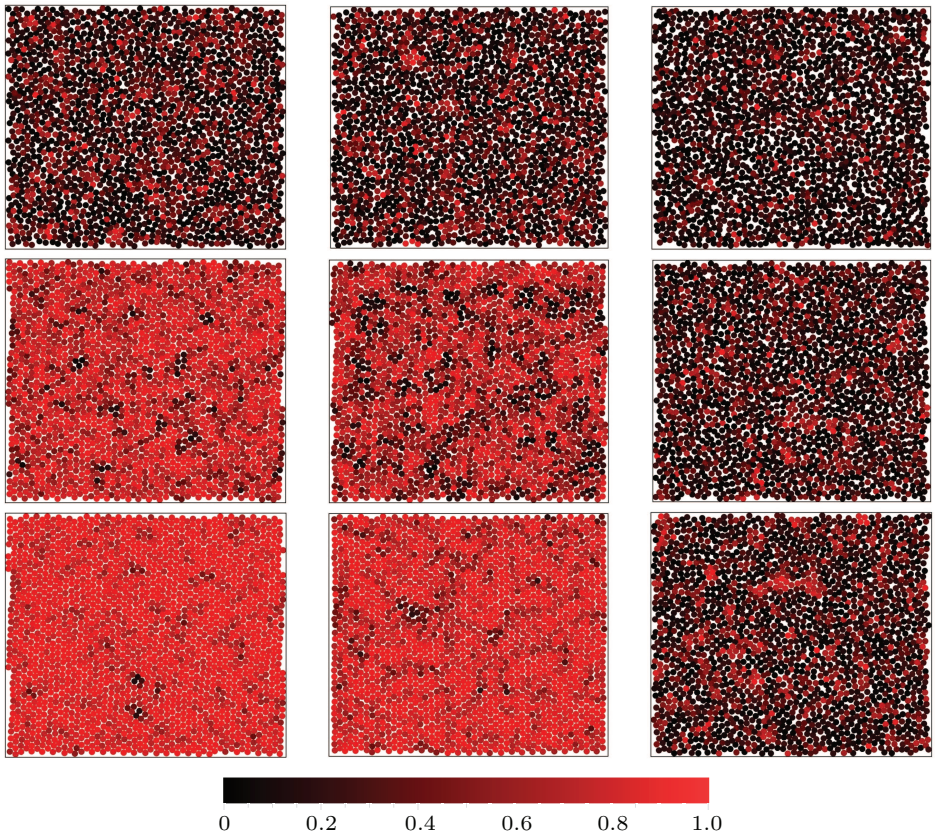


Fig. 4. Snapshots of particle configurations for $\Delta\mu = 0$ (left column), 0.5 (middle column) and 0.9 (right column), the rows correspond to constant Γ, from top to bottom $\Gamma = 200$ (0.2886, 0.2806, 0.2014), 700 (0.7436, 0.6160, 0.2636) and 1400 (0.8627, 0.8128, 0.2982). Particles are colored according to their $\bar{q}_6$.

To assess in more detail the phase transition, we consider a process of melting starting from a perfect hexagonal crystal (dashed lines in Fig. 2), and introduce the Lindemann-like parameter[41]

$$\gamma_{\rm L}(t) \equiv \frac{\left\langle \left|\Delta \boldsymbol{r}_i(t) - \Delta \boldsymbol{r}_j(t)\right|^2 \right\rangle}{2\ell^2} \tag{9}$$

as a criterion to decide the upper bound to solid region. Here, the subscripts i and j denote two particles that are initially neighbors, and the lattice spacing of the hexagonal crystal $\ell \equiv 2^{1/2}3^{-1/4} \simeq 1.075$. This criterion states that the melting commences once the vibrational displacement of a particle exceeds a certain fraction of the lattice spacing.[18] In our case, both the small coupling strength and large diffusion anisotropic degree can induce particles to vibrate sharply, the former has been explicated in Ref. [18]. We now mainly focus on the time dependence of the Lindemann-like parameter for different $\Delta\mu$ at a given Γ, e.g., $\Gamma = 1000$ as shown in Fig. 5(a). It is found that, in the liquid region, the curves of the Lindemann-like parameter are abruptly divergent over time. Especially for $\Delta\mu > 0.65$, due to the existence of intensive diffusion in a special direction, the particles easily escape from their lattice position, and the crystal structure is destroyed. When $\Delta\mu = 0.6$, one can find a quasi-plateau with Lindemann-like parameter $\gamma_{\rm L}$, we define this value $\Delta\mu_{\rm L}^*$ as the melting point. Based on the above description, the phase diagram is mapped in Fig. 5(b). Clearly, the curves of $\Delta\mu_{\rm S}^*$ and $\Delta\mu_{\rm D}^*$ mostly coincide in all parameter space, which indicates that the two criterions we employed are compatible with our model. Note that in the region with large Γ and small $\Delta\mu$, the particles crystalize into hexagonal structures, whereas in the small Γ or large $\Delta\mu$ region, the bond-orientational order is destroyed due to long-time diffusion. Moreover, there is a transition regime between liquid and solid, which is characterized by a high structural order and low but non-vanishing diffusion.[18] It is clear that the transition regime widens in the region of moderate parameter space, we regard it as the result of the competition between the degree of diffusion anisotropy and coupling strength, as shown in Fig. 2.

We begin from briefly review our results to characterize the solid, liquid and transition regions. Figure 6(a) illustrates the probability distribution for $\bar{q}_6$ with different Γ at $\Delta\mu = 0.5$. One can find that the system is less structured in liquid region ($\Gamma = 200$), while in the solid region ($\Gamma = 1400$), the particles are well-crystallized with a few "bubbles" due to the long-range bond-orientational order. Notably, for the transition region ($\Gamma = 700$), there is a broad peak probability distribution for $\bar{q}_6$, corresponding to a coexistence phase as the second snapshot of middle column shown in Fig. 4. Figure 6(b) displays the probability distributions of $\bar{q}_6$ at $\Delta\mu = 0$, 0.5 and 0.9

for four different global ψ_6 values. As has mentioned, when $\Delta\mu = 0.9$, the system is always disordered ($\psi_6 < 0.3$), thus there is only one curve. One can easily find that the probability distributions of $\bar{q}_6$ are less dependent on $\Delta\mu$. It should be emphasized that a quasi-platform stretches across the distribution curve of $\psi_6 = 0.45$, which means that the transition regime is occupied by a variety of heterogeneous structures.

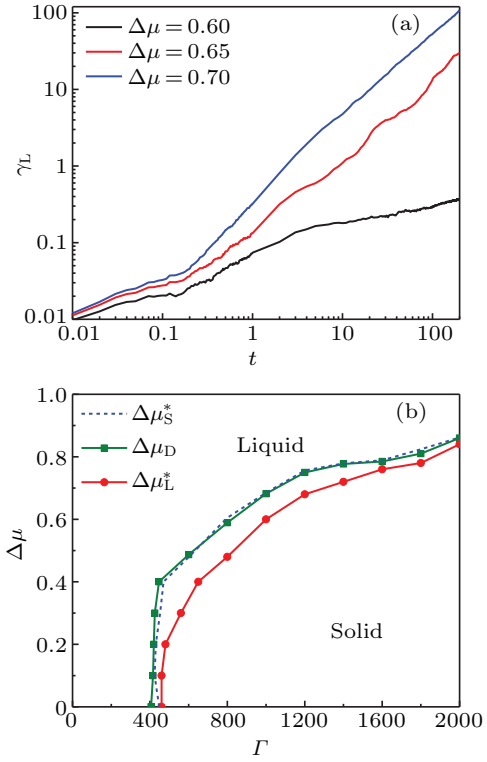


Fig. 5. (a) Time dependence of the Lindermann parameter for $\Gamma = 1000$. (b) Phase diagram in the Γ–$\Delta\mu$ plane.

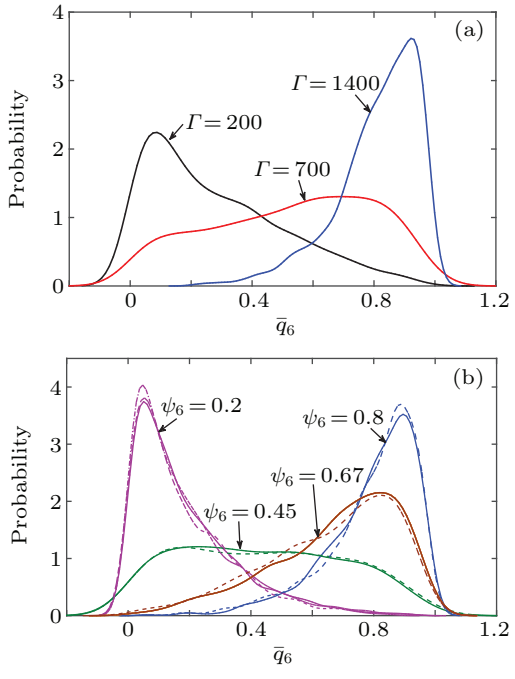


Fig. 6. Probability distributions of $\bar{q}_6$ (a) for different Γ at $\Delta\mu = 0.5$ and (b) at $\Delta\mu = 0$ (solid line), 0.5 (dashed line) and 0.9 (dot-dashed line) for four different global ψ_6 values.

4. Concluding remarks

To summarize, we have numerically studied the solid-liquid phase transition in a dense suspension of spherical colloids with different diffusions in an orthogonal direction. Starting from a random particle configuration, we have simulated the Langivin equations using the second-order stochastic Runge–Kutta algorithm in a two-dimensional box under periodic boundary conditions. The results show that the phase transition is strongly dependent on the diffusion anisotropy of colloidal particles. In the case of high temperature, a large diffusion anisotropic degree can induce particles to vibrate sharply, escape from the lattices, and destroy the long-range bond-orientational order. As a result, the process of crystallization is prevented. Furthermore, the strong-coupled particles with weak anisotropic diffusion can freeze into hexagonal crystals. By employing different criteria, the phase diagram in the Γ–$\Delta\mu$ plane is obtained. It is clear that for a large $\Delta\mu$ or small Γ regime, the system always keeps liquid phase. However, the particles with small $\Delta\mu$ and large Γ are easily frozen into solid. There exists a transition region in which the suspension is overall ordered but with quite a few heterogeneous structures, which reflects as a broad-peak distribution for $\bar{q}_6$. A competition between $\Delta\mu$ and Γ widens this region in the moderate parameter space.

Acknowledgements

Project supported in part by the National Natural Science Foundation of China (Grant Nos. 12075090, 11905086 and 12165015), the GDUPS (2016), and the Major Basic Research Project of Guangdong Province, China (Grant No. 2017KZDXM024), and the Natural Science Foundation of Jiangxi Province, China (Grant Nos. 2021BAB201015 and GJJ200820), and Science and Technology Planning Project of Ganzhou City (Grant No. 202101095077), and High-level Scientific Research Foundation for the Introduction of Talents of Jiangxi University of Science and Technology.

References

[1] Li D, Zhou H and Honma I 2004 *Nat. Mater.* **3** 65
[2] Liu H, Kumar S K and Douglas J F 2009 *Phys. Rev. Lett.* **103** 018101
[3] Lin H X, Lee S, Sun L, Spellings M, Engel M, Glotzer S C and Mirkin C A 2017 *Science* **355** 931
[4] Zaccarelli E, Valeriani C, Sanz E, Poon W C K, Cates M E and Pusey P N 2009 *Phys. Rev. Lett.* **103** 135704
[5] Sanz E, Valeriani C, Zaccarelli E, Poon W C K, Pusey P N and Cates M E 2011 *Phys. Rev. Lett.* **106** 215701
[6] Ni R, Cohen Stuart M A, Dijkstra M and Bolhuis P G 2014 *Soft Matter* **10** 6609
[7] Briand G and Dauchot O 2016 *Phys. Rev. Lett.* **117** 098004
[8] Nie P, Chattoraj J, Piscitelli A, Doyle P and Ciamarra M P 2020 *Phys. Rev. Res.* **2** 023010
[9] Auer S and Frenkel D 2002 *J. Phys.: Condens. Matter* **14** 7667
[10] Reinke D, Stark H, von Grünberg H H, Schofield A B, Maret G and Gasser U 2007 *Phys. Rev. Lett.* **98** 038301

[11] Smallenburg F, Boon N, Kater M, Dijkstra M and van Roij R 2011 *J. Chem. Phys.* **134** 074505
[12] Anderson V J and Lekkerkerker H N W 2002 *Nature* **416** 811
[13] Poon W C K 2002 *J. Phys.: Condens. Matter* **14** R859
[14] Frenkel D 2002 *Science* **296** 65
[15] Kose A, Ozaki M, Takano K, Kobayashi Y and Hachisu S 1973 *J. Colloid Interface Sci.* **44** 330
[16] Crocker J C and Grier D G 1996 *J. Colloid Interface Sci.* **179** 298
[17] Yin Q Q, Li Y Y, Marchesoni F, Debnath D and Ghosh P K 2021 *Chin. Phys. Lett.* **38** 040501
[18] Bialké J, Speck T and Löwen H 2012 *Phys. Rev. Lett.* **108** 168301
[19] Lei L, Wang S, Zhang X, Lai W J, Wu J Y and Gao Y X 2020 *Chin. Phys. B* **30** 056112
[20] Allahyarov E, Sandomirski K, Egelhaaf S U and Löwen H 2015 *Nat. Commun.* **6** 7110
[21] Li B, Zhou D and Han Y 2016 *Nat. Rev. Mater.* **1** 15011
[22] Singh D P, Choudhury U, Fischer P and Mark A G 2017 *Adv. Mater.* **29** 1701328
[23] Briand G, Schindler M and Dauchot O 2018 *Phys. Rev. Lett.* **120** 208001
[24] Valeriani C, Sanz E, Zaccarelli E, Poon W C K, Cates M E and Pusey P N 2011 *J. Phys. Condens. Matter* **23** 194117
[25] Schofield A B, Pusey P N and Radcliffe P 2005 *Phys. Rev. E* **72** 031407
[26] Schaertl N, Botin D, Palberg T and Bartsch E 2018 *Soft Matter* **14** 5130
[27] Velasco E, Navascués G and Mederos L 1999 *Phys. Rev. E* **60** 3158
[28] Hynninen A P, Filion L and Dijkstra M 2009 *J. Chem. Phys.* **131** 064902
[29] Dijkstra M 2014 *Adv. Chem. Phys.* **156** 35
[30] Ai B Q and Wu J C 2014 *J. Chem. Phys.* **140** 094103
[31] Liao J J, Zhu W J and Ai B Q 2018 *Phys. Rev. E* **97** 062151
[32] Jin W, Chan H K and Zhong Z 2020 *Phys. Rev. Lett.* **124** 248002
[33] Han Y, Alsayed A M, Nobili M, Zhang J, Lubensky T C and Yodh A G 2006 *Science* **314** 626
[34] Han Y, Alsayed A, Nobili M and Yodh A G 2009 *Phys. Rev. E* **80** 011403
[35] Kawamura H 1981 *Prog. Theor. Phys.* **66** 772
[36] Halperin B I and Nelson D R 1978 *Phys. Rev. Lett.* **41** 121
[37] Schweigert I V, Schweigert V A and Peeters F M 1999 *Phys. Rev. Lett.* **82** 5293
[38] Löwen H 1996 *Phys. Rev. E* **53** R29
[39] Hartmann P, Kalman G J, Donko Z and Kutasi K 2005 *Phys. Rev. E* **72** 026409
[40] Lechner W and Dellago C 2008 *J. Chem. Phys.* **129** 114707
[41] Zahn K and Maret G 2000 *Phys. Rev. Lett.* **85** 3656